*Acta Cryst.* (1997). B53, 102–112

# Distortion Characteristics Across the Structural Phase Transition in $(Cu_{1-x}Zn_x)WO_4$

PAUL F. SCHOFIELD,[a]* K. S. KNIGHT,[b] S. A. T. REDFERN[c] AND G. CRESSEY[a]

[a]*Department of Mineralogy, The Natural History Museum, Cromwell Road, London SW7 5BD, England,* [b]*ISIS Science Division, Rutherford Appleton Laboratory, Didcot, Oxfordshire OX11 0QX, England, and* [c]*Department of Earth Sciences, University of Cambridge, Downing Street, Cambridge CB2 3EQ, England. E-mail: pfs@uhm.ac.uk*

*(Received 20 May 1996; accepted 18 September 1996)*

## Abstract

Rietveld analysis of neutron powder diffraction data on the sanmartinite ($ZnWO_4$)–cuproscheelite ($CuWO_4$) solid solution has enabled the comparison of microscopic and macroscopic order parameters associated with the $P2/c$–$P\bar{1}$ structural phase transition. The macroscopic spontaneous strain, calculated from the lattice parameters, conforms well with a second-order Landau model. Furthermore, this is also true of the symmetry-related atomistic $M$—O order parameter and the quadratic elongation of the $MO_6$ octahedra. It is clear that the Jahn–Teller effect, associated with the divalent Cu cation, is the driving force for the phase transition and the excess elongation evident in the $M$—O(2) bond giving rise to the non-symmetry predicted strain element $e_{22}$. The existence of a large region of order parameter saturation at the copper-rich end of the solid solution is also associated with the $MO_6$ elongation and the breakdown of the homogeneous strain field of the zinc solute atoms.

## 1. Introduction

Sanmartinite ($ZnWO_4$) and cuproscheelite ($CuWO_4$) are both members of the wolframite series of structurally related materials. Several divalent transition-metal tungstates of the form $MWO_4$ have been characterized as wolframite-type tungstates, also referred to as $NiWO_4$-type, and in these instances $M$ = Mg, Mn, Fe, Co, Ni, Zn, Cd and Cu. In these materials both the $M$ cations and tungsten ions reside on non-equivalent octahedral sites.

Crystals of both $ZnWO_4$ and $CuWO_4$ have attracted a great deal of scientific interest principally due to their potential technological importance as scintillation detectors, photoanodes and within microwave devices. Arora, Mathew & Batra (1988) and Foldvari *et al.* (1986) have explored the growth of end-member single crystals, and the charge balancing characteristics of $OH^-$ ions in such crystals have been assessed by Foldvari, Capelletti, Kappers, Gilliam & Watterich (1989). Elastic, acoustic (Pisorevskii *et al.*, 1988) and optical (Scott, 1968; Arora, Mathew & Batra, 1989) properties have been measured and various electrical properties such as the dielectric constants (Brower, 1970; Arora & Mathew, 1989), the electronic and ionic conductivities (Moebius, Witzmann & Harzer, 1963; Bharati, Singh & Yadava, 1983; Mathew, Batra & Arora, 1992) and cathodic properties (di Pietro, Scrosati, Bonino & Lazzari, 1979) have been well characterized. Photochemical (Benko & MacLaurin, 1982; Arora, Mathew & Batra, 1990), reduction (Basu & Sale, 1978, 1979) and scintillation (Zhu *et al.*, 1986) properties have all been explored and the magnetic structures and susceptibilities (Shapovalova, Belova, Zalesskii & Gerasimov, 1961; Doumerc, Dance, Chaminade, Pouchard & Hagenmuller, 1981; Forsyth, Wilkinson & Zvyagin, 1991) well defined.

While properties of tungstate crystals containing small amounts of various chemical dopants on both the $M$ site and the W site have been much studied, the properties and possible exploitation of mixed crystals in the $(Cu_{1-x}Zn_x)WO_4$ system have still to be assessed. Indeed, the only study of such properties, involving a significant degree of solid solution, was that of Zvyagin & Anders (1974) who monitored the magnetic ordering as a function of temperature for $(Cu_xZn_{1-x})WO_4$, where $1 \geq x \geq 0.8$.

## 2. Crystal structures

The structure of $ZnWO_4$ (Fig. 1*a*) was initially solved by Filipenko, Pobedimskay & Belov (1968) from X-ray diffraction data, showing it to be isostructural with the monoclinic ($P2/c$) wolframite structure, and later refined by Schofield, Knight & Cressey (1996) using neutron diffraction. The structure comprises infinite zigzag chains, running parallel to [001], of either edge-sharing $ZnO_6$ octahedra or edge-sharing $WO_6$ octahedra. Each chain of $ZnO_6$ octahedra is corner-linked to four chains of $WO_6$ octahedra and *vice versa*, leaving open channels which are also parallel to [001]. Within the network of hexagonally close-packed O atoms the Zn and W atoms are ordered on the octahedral interstices such that layers of O,W,O,Zn,O... are formed, and these are interlayered with cation-absent layers. The $ZnO_6$ and $WO_6$ octahedra consist of three pairs of cation—oxygen

bonds with the Zn and W atoms being displaced from the centre of their octahedra by approximately 0.29 and 0.32 Å, respectively, along [010].

The structure of $CuWO_4$ (Fig. 1*b*) was first solved by Kihlborg & Gebert (1970) and later refined by Klein & Weitzel (1975). Whilst studying the antiferromagnetic ordering of $CuWO_4$ below 23 K, Forsyth, Wilkinson & Zvyagin (1991) refined the structure at 4 K; it showed little change in the fractional coordinates with those of the single crystal X-ray study of Kihlborg & Gebert (1970). The structure of $CuWO_4$ is topologically identical to that of the wolframite structure, however, the significant Jahn–Teller effect from the $Cu^{2+}$ cation lowers the degeneracy of the 3*d* orbitals and results in an axial elongation of the $CuO_6$ octahedra. Thus, although the site symmetry of the $Cu^{2+}$ cation is $\bar{1}$, the $CuO_6$ octahedra possess a pseudo-tetragonally elongated geometry, with four O atoms in an approximate square planar configuration at a mean Cu—O bond distance of 1.98 Å and two axial Cu—O bonds at approximately 2.4 Å. The geometrical off-centring of the W atoms within their octahedra is ~0.24 Å. Overall these effects lower the monoclinic symmetry and lead to the space group $P\bar{1}$, with a large triclinic distortion reflected by the deviation of the $\alpha$ and $\gamma$ angles from 90°.

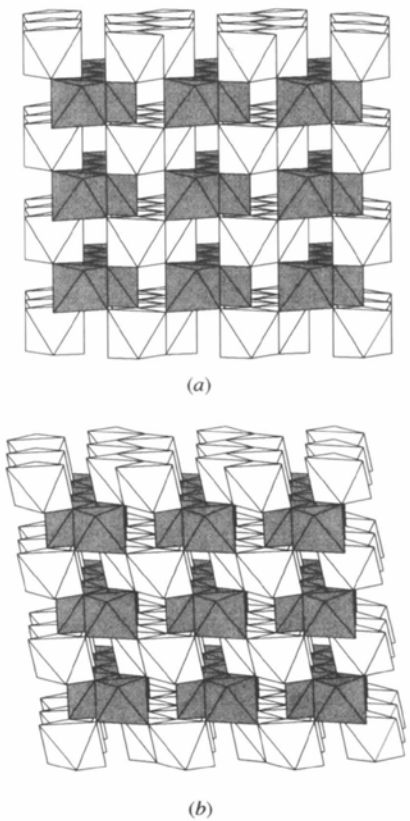

(*a*)

(*b*)

Fig. 1. The crystal structures of (*a*) $ZnWO_4$ and (*b*) $CuWO_4$.

## 3. Structural phase transition

Complete solid solution between sanmartinite and cuproscheelite was demonstrated by Schofield & Redfern (1992) who measured the lattice parameters of samples at 5 mol% intervals across the series using high-resolution Guinier X-ray diffraction. The lattice parameters vary continuously and reveal a structural phase transition between the $P2/c$ and the $P\bar{1}$ structures at a composition close to $Zn_{0.78}Cu_{0.22}WO_4$. The same $P2/c$–$P\bar{1}$ phase transition is also observed as a function of temperature for samples with a Zn content of $x < 0.78$ (Schofield & Redfern, 1993). This temperature-induced phase transition changes character from second-order through tricritical, at approximately $Zn_{0.68}Cu_{0.32}WO_4$ to first-order on increasing the Cu content. The symmetry-adapted spontaneous strain within the triclinic phases, which amounted to some 6.5% in the $CuWO_4$ end-member, was used as a measure of the order parameter for the transition. Subsequently, the thermodynamic behaviour of the ferroelastic phase transition was successfully modelled by a Landau potential.

Some microscopic structural distortions across the phase transition in the $(Cu_{1-x}Zn_x)WO_4$ series have also been investigated by X-ray absorption techniques (Schofield, Henderson, Redfern & van der Laan, 1993; Schofield, Charnock, Cressey & Henderson, 1994). Cu 2*p* absorption spectroscopy identified the existence of two distinct Cu electronic environments in the mixed crystals, whereas only one is evident in the $CuWO_4$ end-member. These two environments both showed an increase in covalency as the Cu content increased and were associated with the presence/absence of $ZnO_6$ neighbours adjacent to $CuO_6$ octahedra. It was concluded that the difference in electronic structure between the two environments was due to either a shortening of the tetragonally elongated Cu—O bond or to changes in the proportions of the ground states $2p^63d^9$ and $2p^63d^{10}\underline{L}$, of the Cu atoms. Modelling of the occupancies across the series clearly showed a dependency upon the structural state of the crystal and as such the occupancies altered greatly near the critical composition of the $P2/c$–$P\bar{1}$ phase transition. Cu *K*-edge EXAFS (extended X-ray absorption fine structure) across the series implied that only a single geometrical Cu site, axially elongated, was present in the majority of the $(Cu_{1-x}Zn_x)WO_4$ series and hence could not determine the nature of the two distinct electronic Cu sites indicated from the Cu 2*p* spectra. The atomic environments beyond the first coordination shell did, however, show significant variation leading up to the critical composition. Zn *K*-edge EXAFS, on the other hand, revealed that the introduction of Cu into $ZnWO_4$ generated two structurally distinct $ZnO_6$ octahedra, one containing two short Zn—O bonds and four long Zn—O bonds, as in $ZnWO_4$, and one

mimicking the axially elongated geometry of the $CuO_6$ octahedra in $CuWO_4$. The proportions of these two sites were found to vary as a function of Cu content and an increase in the degree of octahedral distortion was evident at the critical composition.

The phase transition is associated with an instability at the centre of the Brillouin zone, but is not related to simple distortions of a framework of rigid octahedra (Redfern, Bell, Henderson & Schofield, 1995). Instead, the driving force for the transitions is the cooperative Jahn–Teller distortion of the $CuO_6$ octahedra, while the $WO_6$ and $ZnO_6$ octahedral distortions may essentially be regarded as a secondary process (Redfern, 1993; Redfern, Bell, Henderson & Schofield, 1995). While the studies of the long-range and short-range behaviour are clearly complementary, there still remain unanswered some intriguing physical and crystallographic questions. For example, the existence, or otherwise, of two subtly different sets of $CuO_6$ octahedra within the mixed crystals has yet to be demonstrated by structural crystallographic methods and a question remains as to whether or not these two distinct Cu electronic environments are structurally induced. The existence of two geometrically distinct sets of $CuO_6$ and $ZnO_6$ octahedra in the mixed crystals, but not in the end-member crystals, would necessitate a decrease in macroscopic symmetry for the intermediate samples, or alternatively may induce a cell doubling. Also, the possibility of ordering or clustering of like and/or dislike octahedra must be explored and correlated, if possible, to the structural behaviour displayed. In this paper we have employed the advantages of neutron powder diffraction and Rietveld refinement in an attempt to resolve these problems and to relate the microscopic distortion patterns to the macroscopic order parameters for the $(Cu_{1-x}Zn_x)WO_4$ system.

## 4. Synthesis and characterization

Samples were synthesized at 5 mol% intervals across the composition range from $ZnWO_4$ to $CuWO_4$ using a direct synthesis method described in detail elsewhere (Schofield & Redfern, 1992). This method has also been successful for the scheelite–powellite solid solution, $Ca(Mo_xW_{1-x})O_4$ (Shoji & Sasaki, 1978; Tyson, Hemphill & Theisen, 1988). Precipitates, formed from mixing solutions containing stoichiometric amounts of $CuSO_4.5H_2O$, $ZnSO_4.7H_2O$ and $Na_2WO_4.2H_2O$, were dried and washed before being ground in an agate pestle and mortar and annealed under atmospheric conditions at 873 K for 88 h.

The samples are identical to those used in the studies on this system described in the previous section and as such have been well characterized. Chemical analysis was performed using wavelength-dispersive EPM (electron-probe microanalysis) and energy-dispersive ATEM (analytical transmission electron microscopy) analysis. No signs of chemical inhomogeneity were observed on the length scale of the transmission electron microscope, although in most of the samples a small amount of CuO was detected as a separate phase, the presence of which is discussed by Redfern, Bell, Henderson & Schofield (1995). The $ZnWO_4$ end-member possesses a small amount of ZnO impurity, which is evident in Fig. 2 and discussed by Schofield, Knight & Cressey (1996). No evidence for significant deviation in the stoichiometry of the samples from that of the compositions reported has been observed in any of the previous studies detailed above, and as such the compositional errors are smaller than the size of the data-point symbols in the figures.

## 5. Neutron diffraction

Neutron time-of-flight powder diffraction data were collected on the medium resolution diffractometer POLARIS (Smith, Hull & Armstrong, 1994) at the ISIS neutron spallation source, Rutherford Appleton Laboratory, England (Wilson, 1995). Diffraction

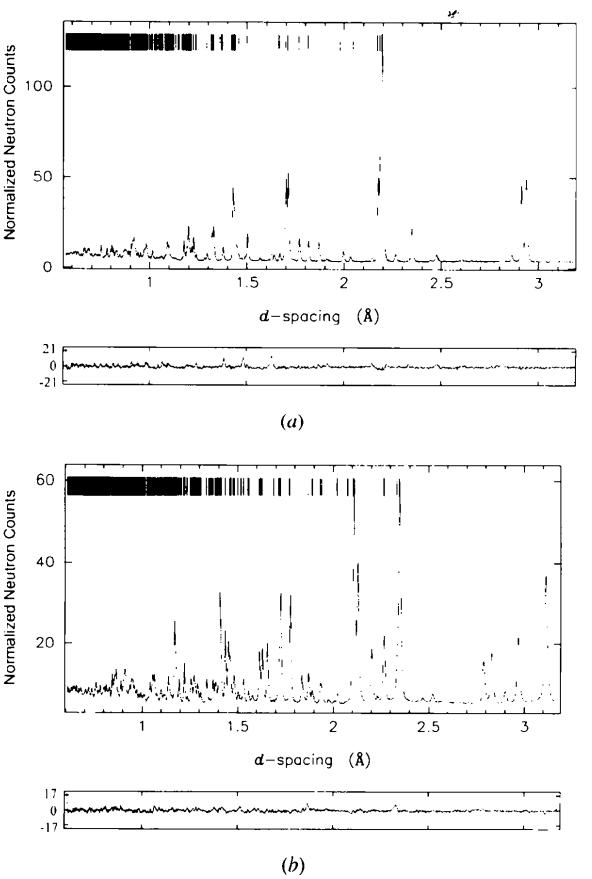


Fig. 2. The neutron powder diffraction profiles for (*a*) $ZnWO_4$ and (*b*) $CuWO_4$ with dots representing the raw data and the solid line representing the Rietveld model. The limits on the residual plots are $\pm 3\sigma$.

patterns were collected for tungstate samples at 5 mol% intervals across the series. Data in the time-of-flight range 3500–19250 μs, corresponding to a $d$-spacing range from 0.56 to 3.89 Å, were binned as $\Delta t/t = 0.001$, background subtracted, corrected for the incident flux distribution and detector efficiency using the isotropic incoherent scattering from a vanadium rod and corrected for absorption and self scattering. These data were subsequently used in Rietveld profile refinement.

## 6. Data refinement

Rietveld profile refinements were carried out using the dedicated time-of-flight package *TF14LS* (David, Ibberson & Matthewman, 1992) based on the Cambridge Crystallographic Subroutine Library. The refinements were performed using the coherent scattering lengths from Sears [1992 (Cu 7.718, Zn 5.680, W 4.86 and O 5.803 fm)] and the starting models were the coordinates of Filipenko, Pobedimskay & Belov (1968) for monoclinic $ZnWO_4$ and of Klein & Weitzel (1975) for triclinic $CuWO_4$. The calculated parameters for the refinement of $ZnWO_4$ were then used as the initial data set for $Cu_{0.05}Zn_{0.95}WO_4$, and so for the subsequent refinements of the monoclinic structures. Similarly, the calculated parameters for the refinement of $CuWO_4$ were used as the initial data set for $Cu_{0.95}Zn_{0.05}WO_4$ and so on for the subsequent refinements of the triclinic structures. Although site occupancies of the Zn and Cu atoms were varied in accordance with the composition of the samples across the series, they were constrained to refine identically. Refinements were tried without these constraints, but are discussed later in §8.

Fig. 2 shows the final fit to the data for $ZnWO_4$ and $CuWO_4$, with the dots representing the diffraction data and the solid line the calculated structure. The residual plot between the diffraction profiles is shown with the horizontal dotted lines reflecting $\pm 3\sigma$. $ZnWO_4$ agreement factors are $R_p = 0.045$, $R_{wp} = 0.037$, $R_E = 0.015$, $\chi^2 = 5.9$ for 1723 observations and 31 variables, and the agreement factors for $CuWO_4$ are $R_p = 0.035$, $R_{wp} = 0.028$, $R_E = 0.015$, $\chi^2 = 3.44$ for 1655 observations and 45 variables.

## 7. Lattice parameters and spontaneous strain

High-precision lattice parameters, extracted from the Rietveld analysis (given in Table 1, displayed in Fig. 3) can be seen to excellently complement those of Schofield & Redfern (1992). As the Cu content increases from the $ZnWO_4$ end-member, the lattice constant $a$ decreases almost linearly up to $X_c$, $(Cu_{0.22}Zn_{0.78})WO_4$, and then increases as the triclinic distortion increases. There is a clear deviation at $X_c$ in the linear increase in $b$ and the linear decrease in $c$, as the Cu content is increased, however, there is no change in sign of the gradients. The cell angles $\alpha$ and $\gamma$ behave as expected, with the large triclinic distortion evident from the large deviations from 90°, particularly of $\gamma$. As the Zn content is increased, the $\beta$ angle, which is not directly involved with the $P2/c$–$P\bar{1}$ transition, does, however, decrease continuously across the entire series. Although orthorhombic symmetry is closely approached at the Zn end of the series, no such transition occurs. The unexpected but significant excess volume within the triclinic phase, which had to be accounted for in the Landau model of Schofield & Redfern (1992), is also clearly evident.

The symmetry-adapted spontaneous strain tensor generated in the low-symmetry phase only requires the components $e_{12}$ and $e_{23}$, containing $\alpha$ and $\gamma$, which can be calculated from the lattice parameters using the equations of Redfern & Salje (1987). Based on symmetry arguments alone no transition-dependent behaviour in the $b$ lattice parameter is expected for this system. Fig. 3, however, clearly shows that this is not the case, and as such this behaviour of $b$ is responsible for the existence of the strain component $e_{22}$. These strain components, along with the overall spontaneous strain, are shown in Fig. 4. Again, the continuous nature of the structural phase transition as a function of composition is evident from these strain

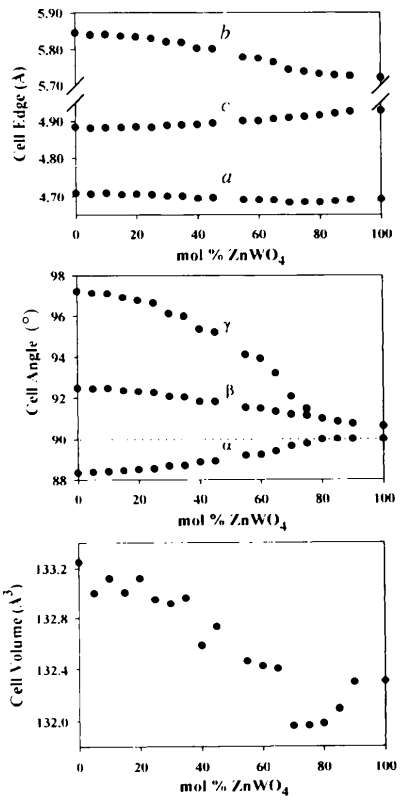


Fig. 3. The variation of the lattice parameters extracted from the Rietveld analyses, as a function of composition.

Table 1. *Lattice parameters (Å, °, Å³) for $(Cu_{1-x}Zn_x)WO_4$ obtained from the Rietveld analyses*

| Mol% Zn | *a* | *b* | *c* | *α* | *β* | *γ* | *V* |
|---|---|---|---|---|---|---|---|
| 100 | 4.69263 (5) | 5.72129 (7) | 4.92805 (5) | 90 | 90.6321 (9) | 90 | 132.300 (2) |
| 90 | 4.69114 (6) | 5.72608 (7) | 4.92536 (6) | 90 | 90.7507 (9) | 90 | 132.293 (3) |
| 85 | 4.68766 (8) | 5.72752 (10) | 4.92052 (8) | 90 | 90.8566 (13) | 90 | 132.095 (4) |
| 80 | 4.68502 (5) | 5.73194 (7) | 4.91560 (5) | 90 | 91.0026 (9) | 90 | 131.985 (3) |
| 75 | 4.68499 (11) | 5.73796 (16) | 4.91163 (12) | 89.766 (2) | 91.135 (2) | 91.467 (2) | 131.966 (6) |
| 70 | 4.68411 (10) | 5.74374(13) | 4.90925 (10) | 89.6303 (19) | 91.1899 (18) | 92.0730 (18) | 131.963 (5) |
| 65 | 4.69010 (9) | 5.76474 (10) | 4.90647 (8) | 89.3597 (14) | 91.3394 (13) | 93.2364 (13) | 132.403 (4) |
| 60 | 4.69097 (9) | 5.77510 (9) | 4.90169 (7) | 89.2071 (13) | 91.4870 (12) | 93.9239 (13) | 132.425 (4) |
| 55 | 4.69174 (12) | 5.77857 (13) | 4.90054 (9) | 89.1685 (17) | 91.5190 (16) | 94.1000 (16) | 132.464 (5) |
| 45 | 4.69651 (18) | 5.80159 (18) | 4.89491 (11) | 88.913 (2) | 91.8172 (19) | 95.215 (2) | 132.733 (8) |
| 40 | 4.6947 (3) | 5.8028 (3) | 4.89158 (16) | 88.871 (3) | 91.828 (3) | 95.367 (3) | 132.588 (11) |
| 35 | 4.70189 (19) | 5.81866 (18) | 4.89057 (11) | 88.706 (2) | 92.0510 (19) | 95.982 (2) | 132.962 (8) |
| 30 | 4.7013 (4) | 5.8207 (4) | 4.8890 (2) | 88.678 (4) | 92.073 (4) | 96.099 (4) | 132.917 (16) |
| 25 | 4.70508 (13) | 5.82979 (11) | 4.88441 (7) | 88.5414 (13) | 92.2845 (12) | 96.6112 (13) | 132.952 (5) |
| 20 | 4.70707 (19) | 5.83407 (18) | 4.88649 (10) | 88.511 (2) | 92.3254 (17) | 96.7350 (19) | 133.124 (8) |
| 15 | 4.70559 (12) | 5.83597 (10) | 4.88391 (6) | 88.4601 (12) | 92.3623 (10) | 96.8837 (11) | 133.008 (5) |
| 10 | 4.7095 (2) | 5.84030 (19) | 4.88323 (11) | 88.413 (2) | 92.5035 (18) | 97.095 (2) | 133.122 (9) |
| 5 | 4.70682 (11) | 5.83985 (10) | 4.88214 (6) | 88.3889 (11) | 92.4646 (10) | 97.1148 (10) | 133.004 (5) |
| 0 | 4.70953 (16) | 5.84516 (14) | 4.88492 (8) | 88.3530 (16) | 92.5081 (14) | 97.2047 (15) | 133.246 (7) |

calculations. The extra strain component $e_{22}$ is likely to be responsible for, or at the very least significantly contribute towards, the excess volume present in the low-symmetry tungstates. The possible origins of this strain are discussed, later, in the light of the assessments of the microscopic structural changes gleaned from the Rietveld analyses.

## 8. Multi-site considerations

Previous studies on the structure of $CuWO_4$, discussed earlier, have attempted refinements in the lower symmetry of $P\bar{1}$. In each case, however, no conclusive evidence was found to justify any space group other than $P\bar{1}$. The existence of two sets of geometrically distinct $ZnO_6$ octahedra and $CuO_6$ octahedra in the intermediate $(Cu_xZn_{1-x})WO_4$ samples, as implied by the spectroscopic studies, would necessitate either a reduction in the macroscopic symmetry or a doubling of the unit cell. We tried several structural refinements for some of the intermediate triclinic samples in lower symmetry than $P\bar{1}$ and with an increased number of Cu/Zn sites. In every case the final refinement statistics showed no justification for the vastly increased number of parameters of the structural model. Furthermore, for a sensible solution to be obtained, constraints had to be placed on the refinement itself. Doubling the size of the unit cell along each axis also showed no improvement in the fitting statistics and in addition there were no measured peaks consistent with these unit cells. It appears that the microscopic structural changes that are implied by the XAS studies are just too subtle and complex to observe by Rietveld analysis within the $(Cu_xZn_{1-x})WO_4$ system, or do not correspond to long length-scale correlated behaviour.

An assessment of the veracity of the multi-site model may be achieved indirectly by monitoring the variation of the atomic displacement parameters (isotropic *B* value, where $B = 8\pi^2 U$), given in Table 2 and displayed graphically in Fig. 5, particularly for the O atoms O(3) and O(2) which are associated with the Jahn–Teller elongation. The *B* values for the $M^{2+}$ and the $W^{6+}$ cations are fairly constant, although that for the $W^{6+}$ cation does show a reasonable degree of scatter about a horizontal mean. As far as the *B* values for the O atoms are concerned, it is clear that the trend for O(3) is significantly different from that of the others. The *B*

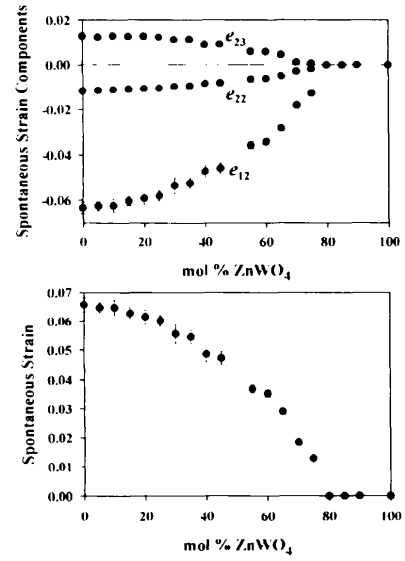


Fig. 4. Spontaneous strain components $e_{12}$, $e_{22}$ and $e_{23}$ and the scalar spontaneous strain, calculated from the equations of Redfern & Salje (1987), associated with the $P2/c$–$P\bar{1}$ structural phase transition.

Table 2. *Atomic coordinates and isotropic displacement parameters ($Å^2$) for $(Cu_{1-x}Zn_x)WO_4$ obtained from the Rietveld analyses*

| Mol% | | *M* | | | | W | | |
|---|---|---|---|---|---|---|---|---|
| $ZnWO_4$ | *x* | *y* | *z* | $B_{iso}$ | *x* | *y* | *z* | $B_{iso}$ |
| 100 | 1/2 | 0.6833 (4) | 1/4 | 0.42 (3) | 0.0 | 0.1823 (5) | 1/4 | 0.22 (4) |
| 90 | 1/2 | 0.6823 (6) | 1/4 | 0.49 (5) | 0.0 | 0.1819 (5) | 1/4 | 0.35 (5) |
| 85 | 1/2 | 0.6810 (7) | 1/4 | 0.38 (6) | 0.0 | 0.1805 (9) | 1/4 | 0.33 (7) |
| 80 | 1/2 | 0.6808 (5) | 1/4 | 0.48 (4) | 0.0 | 0.1811 (6) | 1/4 | 0.23 (5) |
| 75 | 0.4974 (14) | 0.6824 (10) | 0.2485 (14) | 0.57 (7) | −0.0040 (18) | 0.1767 (13) | 0.2522 (19) | 0.32 (9) |
| 70 | 0.5001 (12) | 0.6808 (9) | 0.2542 (13) | 0.44 (7) | −0.0068 (16) | 0.1760 (11) | 0.2457 (15) | 0.16 (9) |
| 65 | 0.4989 (10) | 0.6772 (8) | 0.2578 (10) | 0.42 (7) | −0.0094 (13) | 0.1774 (10) | 0.2488 (12) | 0.19 (8) |
| 60 | 0.4976 (9) | 0.6764 (8) | 0.2597 (10) | 0.40 (6) | −0.0076 (12) | 0.1779 (9) | 0.2479 (12) | 0.16 (7) |
| 55 | 0.4953 (10) | 0.6776 (8) | 0.2599 (10) | 0.37 (6) | −0.0065 (13) | 0.1780 (10) | 0.2483 (12) | 0.05 (8) |
| 45 | 0.5014 (12) | 0.6725 (8) | 0.2590 (12) | 0.55 (7) | −0.0087 (16) | 0.1742 (10) | 0.2478 (14) | 0.30 (9) |
| 40 | 0.4996 (16) | 0.6712 (11) | 0.2578 (16) | 0.49 (9) | −0.011 (2) | 0.17659 (13) | 0.2484 (19) | 0.19 (12) |
| 35 | 0.5047 (11) | 0.6685 (7) | 0.2554 (11) | 0.68 (7) | −0.0153 (12) | 0.1720 (8) | 0.2466 (12) | 0.17 (8) |
| 30 | 0.5042 (12) | 0.6669 (7) | 0.2551 (18) | 0.69 (8) | −0.0160 (14) | 0.1722 (9) | 0.2465 (14) | 0.27 (9) |
| 25 | 0.5040 (7) | 0.6637 (4) | 0.2553 (7) | 0.48 (4) | −0.0191 (8) | 0.1732 (6) | 0.2461 (8) | 0.25 (5) |
| 20 | 0.5040 (9) | 0.6648 (5) | 0.2551 (9) | 0.44 (6) | −0.0189 (10) | 0.1718 (8) | 0.2443 (10) | 0.13 (6) |
| 15 | 0.5055 (6) | 0.6627 (4) | 0.2552 (7) | 0.41 (4) | −0.0211 (7) | 0.1727 (6) | 0.2450 (8) | 0.19 (5) |
| 10 | 0.5063 (8) | 0.6629 (5) | 0.2557 (8) | 0.48 (5) | −0.0203 (9) | 0.1710 (8) | 0.2428 (11) | 0.26 (6) |
| 5 | 0.5055 (5) | 0.6617 (3) | 0.2561 (5) | 0.45 (3) | −0.02204 (6) | 0.1718 (5) | 0.2447 (7) | 0.33 (4) |
| 0 | 0.5065 (5) | 0.6608 (4) | 0.2555 (6) | 0.39 (4) | −0.0225 (7) | 0.1729 (5) | 0.2447 (8) | 0.36 (4) |

| Mol% | | O(1) | | | | O(2) | | |
|---|---|---|---|---|---|---|---|---|
| $ZnWO_4$ | *x* | *y* | *z* | $B_{iso}$ | *x* | *y* | *z* | $B_{iso}$ |
| 100 | 0.2547 (3) | 0.3772 (3) | 0.4005 (3) | 0.45 (2) | 0.2171 (3) | 0.8955 (3) | 0.4360 (3) | 0.36 (2) |
| 90 | 0.2545 (4) | 0.3781 (4) | 0.4015 (5) | 0.54 (4) | 0.2152 (4) | 0.8945 (4) | 0.4376 (4) | 0.42 (4) |
| 85 | 0.2549 (6) | 0.3782 (5) | 0.4027 (6) | 0.49 (4) | 0.2151 (6) | 0.8938 (5) | 0.4373 (6) | 0.47 (5) |
| 80 | 0.2564 (4) | 0.3779 (4) | 0.4035 (5) | 0.53 (3) | 0.2156 (4) | 0.8949 (4) | 0.4374 (4) | 0.50 (4) |
| 75 | 0.2590 (13) | 0.3796 (11) | 0.4042 (16) | 0.36 (9) | 0.2129 (11) | 0.8929 (10) | 0.4346 (15) | 0.12 (10) |
| 70 | 0.2557 (12) | 0.3809 (10) | 0.3966 (13) | 0.42 (9) | 0.2204 (12) | 0.8998 (9) | 0.4422 (13) | 0.35 (9) |
| 65 | 0.2544 (10) | 0.3814 (8) | 0.3965 (10) | 0.21 (7) | 0.2176 (10) | 0.9020 (8) | 0.4428 (12) | 0.29 (8) |
| 60 | 0.2533 (10) | 0.3804 (8) | 0.3974 (10) | 0.17 (7) | 0.2182 (10) | 0.9031 (8) | 0.4431 (12) | 0.43 (8) |
| 55 | 0.2529 (10) | 0.3787 (8) | 0.3981 (11) | 0.09 (8) | 0.2206 (10) | 0.9041 (9) | 0.4429 (12) | 0.35 (8) |
| 45 | 0.2569 (12) | 0.3822 (11) | 0.4045 (14) | 0.36 (8) | 0.2199 (11) | 0.9068 (10) | 0.4449 (14) | 0.45 (9) |
| 40 | 0.2549 (17) | 0.3763 (14) | 0.3999 (18) | 0.30 (10) | 0.2223 (15) | 0.9071 (14) | 0.4457 (19) | 0.46 (11) |
| 35 | 0.2605 (11) | 0.3826 (10) | 0.4028 (11) | 0.48 (8) | 0.2179 (9) | 0.9106 (9) | 0.4455 (11) | 0.32 (8) |
| 30 | 0.2614 (12) | 0.3821 (10) | 0.4016 (12) | 0.53 (8) | 0.217 (1) | 0.9099 (10) | 0.4466 (13) | 0.40 (10) |
| 25 | 0.2617 (8) | 0.3797 (6) | 0.4020 (7) | 0.42 (5) | 0.2171 (7) | 0.9094 (6) | 0.4462 (8) | 0.30 (6) |
| 20 | 0.2604 (10) | 0.3794 (7) | 0.4018 (9) | 0.38 (6) | 0.2184 (8) | 0.9089 (8) | 0.4461 (10) | 0.25 (7) |
| 15 | 0.2622 (8) | 0.3799 (6) | 0.4020 (7) | 0.36 (5) | 0.2182 (7) | 0.9092 (6) | 0.4464 (8) | 0.25 (6) |
| 10 | 0.2606 (9) | 0.3804 (7) | 0.4028 (9) | 0.37 (6) | 0.2186 (8) | 0.9089 (8) | 0.4468 (9) | 0.27 (7) |
| 5 | 0.26310 (6) | 0.3808 (5) | 0.4020 (6) | 0.38 (4) | 0.2180 (6) | 0.9082 (5) | 0.4471 (6) | 0.48 (5) |
| 0 | 0.2635 (6) | 0.3802 (5) | 0.4015 (6) | 0.39 (4) | 0.2175 (6) | 0.9090 (5) | 0.4465 (6) | 0.41 (5) |

| Mol% | | O(3) | | | | O(4) | | |
|---|---|---|---|---|---|---|---|---|
| $ZnWO_4$ | *x* | *y* | *z* | $B_{iso}$ | *x* | *y* | *z* | $B_{iso}$ |
| 75 | 0.7469 (14) | 0.3804 (11) | 0.1035 (16) | 0.65 (9) | 0.7792 (13) | 0.8971 (12) | 0.0554 (15) | 0.45 (10) |
| 70 | 0.7426 (13) | 0.3721 (11) | 0.0872 (15) | 0.61 (9) | 0.7851 (13) | 0.8892 (12) | 0.064 (1) | 0.68 (10) |
| 65 | 0.7429 (12) | 0.3689 (10) | 0.0843 (14) | 0.64 (7) | 0.7859 (11) | 0.8890 (9) | 0.0686 (12) | 0.434 (8) |
| 60 | 0.7435 (12) | 0.3667 (9) | 0.0825 (13) | 0.72 (8) | 0.7857 (10) | 0.8885 (8) | 0.0689 (10) | 0.40 (7) |
| 55 | 0.7449 (13) | 0.3656 (10) | 0.0816 (14) | 0.69 (8) | 0.7840 (11) | 0.8875 (9) | 0.0703 (11) | 0.389 (7) |
| 45 | 0.7513 (15) | 0.2623 (12) | 0.0808 (15) | 0.68 (8) | 0.7798 (13) | 0.8831 (10) | 0.0697 (13) | 0.58 (10) |
| 40 | 0.7489 (20) | 0.3632 (17) | 0.078 (2) | 0.69 (11) | 0.7790 (18) | 0.8839 (14) | 0.0681 (17) | 0.43 (11) |
| 35 | 0.7474 (13) | 0.3624 (10) | 0.0768 (13) | 0.45 (7) | 0.7831 (11) | 0.8778 (9) | 0.0692 (11) | 0.49 (8) |
| 30 | 0.7469 (14) | 0.3626 (11) | 0.0775 (14) | 0.55 (8) | 0.7819 (11) | 0.8754 (10) | 0.0694 (12) | 0.44 (8) |
| 25 | 0.7498 (8) | 0.3581 (6) | 0.0771 (8) | 0.53 (5) | 0.7849 (7) | 0.8791 (6) | 0.0705 (8) | 0.48 (5) |
| 20 | 0.7487 (10) | 0.3582 (8) | 0.0746 (10) | 0.485 (6) | 0.7830 (9) | 0.8769 (8) | 0.0712 (10) | 0.40 (6) |
| 15 | 0.7150 (8) | 0.3578 (7) | 0.0757 (8) | 0.52 (5) | 0.7841 (7) | 0.8790 (6) | 0.0722 (8) | 0.45 (5) |
| 10 | 0.7497 (9) | 0.3566 (8) | 0.0739 (10) | 0.55 (7) | 0.7843 (9) | 0.8772 (8) | 0.0720 (10) | 0.43 (6) |
| 5 | 0.7514 (6) | 0.3564 (5) | 0.0748 (7) | 0.59 (4) | 0.7839 (6) | 0.8782 (5) | 0.0723 (6) | 0.44 (4) |
| 0 | 0.7527 (7) | 0.3567 (5) | 0.0745 (7) | 0.56 (5) | 0.7845 (6) | 0.8778 (5) | 0.0729 (7) | 0.45 (4) |

values for O(3) are consistently higher than all the others and while the $B$ values for O(1), O(2) and O(4) generally show a scatter about a near horizontal mean, the $B$ value for O(3) shows a positive anomaly from linearity, particularly in the middle of the solid solution. This is the region in which the numbers of both Cu sites, observed by Cu $2p$ XAS, are maximized. If the origin of these two Cu sites is structurally related to a subtle shortening of the Jahn–Teller elongated Cu—O bonds, then a significant variation in the $B$ value for the O atoms associated with this Jahn–Teller elongation may indicate two subtly different oxygen positions. As such the anomaly observed in the $B$ value for O(3) may indicate that this is indeed the case, and thus it is the Cu—O(3) bond that is responsible for the two unique Cu electronic environments observed by Cu $2p$ XAS (Schofield, Henderson, Redfern & van der Laan, 1993).

## 9. Distortion patterns

Rigid unit mode analysis has shown that the $P2/c$–$P\bar{1}$ phase transition involves no polyhedral tilting and cannot proceed without octahedral distortion (Redfern, Bell, Henderson & Schofield, 1995). In the monoclinic $ZnWO_4$ structure both the cations are positioned on the diad axis which runs parallel to the $y$ axis (Schofield, Knight & Cressey, 1996). Consequently, the displacement of these cations from the geometric mean of their octahedra is along this direction in the monoclinic phase. After the symmetry reduction to the triclinic phase, however, the orientation of these cation displacement vectors remains close to the pseudo-diad but their magnitude varies significantly as a function of composition. This is shown in Fig. 6. The off-centring of the $M^{2+}$ cation is fairly constant in the monoclinic phases, but decreases rapidly below the transition as the Cu content increases and the overall distortion of the $MO_6$ octahedra increases. The off-centring of the $W^{6+}$ cation, however, does not significantly vary across the solid solution, although there appears to be a clear change in the composition-dependent trends either side of the critical point. The actual values of the $W^{6+}$ cation displacements are lower than those of Redfern, Bell, Henderson & Schofield (1995), whereas the values for the $M^{2+}$ cations are much closer. This is to be expected, and simply reflects the large scattering factor contrast between O and W for X-rays, which manifests itself as poor light atom location in contrast to the neutron scattering lengths which are comparable in magnitude. Such problems are well known in these tungstate systems and have been shown to be responsible for the erroneous structure solutions of minerals such as russellite, $Bi_2WO_6$ (Knight, 1992).

The distortion of the octahedra in the monoclinic phases is also apparent through the behaviour of the $M$—O bonds (Table 3). The octahedra in the monoclinic phases exhibit point-group symmetry 2 and comprise three pairwise $M$—O (or W—O) bonds, but reduce their symmetry to $\bar{1}$ with six unique $M$—O (or W—O) bonds in the triclinic phases. In Fig. 7 this symmetry-controlled splitting is evident as the pairs of bonds in the monoclinic phases can be seen to produce a total excess bond length in the triclinic phases which reflects the macroscopic order parameter. Also evident from Fig. 7 is a significant excess elongation of the $M$—O(2) bond in the triclinic phases. Whereas the

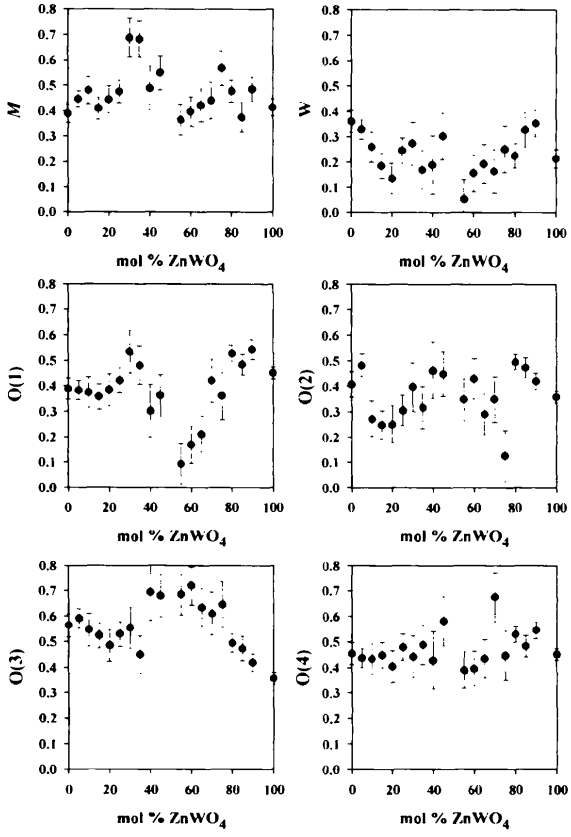


Fig. 5. The variation of the atomic displacement parameters of the $M$, W, O(1), O(2), O(3) and O(4) atoms, showing an anomalously high value for O(3), across the solid solution.

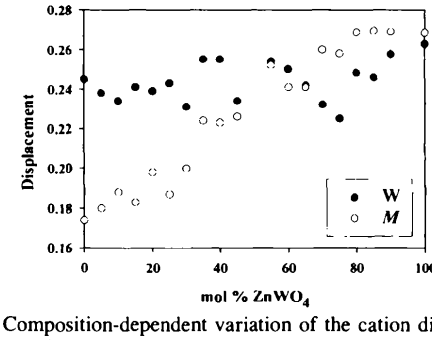


Fig. 6. Composition-dependent variation of the cation displacements (Å) from the nominal centre of the respective octahedra revealing transition-dependent behaviour.

three pairwise W—O bonds split symmetrically in the triclinic phase, it is clear that the $M$—O(1) bond, which splits into $M$—O(2) and $M$—O(4), shows non-symmetrical splitting. The $M$—O(2) bond possesses a large component along the crystallographic $y$ axis, and also forms a nominal axis of elongation with the $M$—O(3) bond of the $CuO_6$ octahedra which is generated by the Jahn–Teller effect. As a consequence, the Jahn–Teller effect upon the $M$—O(2) bond can be confidently assigned responsibility for the unexpected strain component $e_{22}$.*

A second feature to be observed from Fig. 7 is related to the $M$—O(2) bonds, which split into the $M$—O(1$^{i}$) and $M$—O(3$^{iii}$) bonds in the triclinic phase. As the Cu content increases towards the critical composition, the $M$—O(2) bond length in the monoclinic phase

Table 3. *Metal–oxygen octahedral bond distances for* $(Cu_{1-x}Zn_x)WO_4$

| mol% $ZnWO_4$ | $M$—O(1) | $M$—O(1$^{i}$) | $M$—O(2) | | | | W—O(1) | W—O(2$^{ii}$) | W—O(2$^{vi}$) | | | |
|---|---|---|---|---|---|---|---|---|---|---|---|---|
| 100 | 2.227 (3) | 2.090 (2) | 2.026 (2) | | | | 1.790 (2) | 1.915 (2) | 2.133 (3) | | | |
| 90 | 2.222 (3) | 2.084 (3) | 2.037 (2) | | | | 1.795 (2) | 1.902 (2) | 2.135 (3) | | | |
| 85 | 2.217 (3) | 2.073 (5) | 2.039 (2) | | | | 1.802 (3) | 1.901 (1) | 2.129 (3) | | | |
| 80 | 2.217 (3) | 2.061 (6) | 2.043 (2) | | | | 1.804 (3) | 1.904 (1) | 2.128 (3) | | | |
| | $M$—O(1) | $M$—O(2) | $M$—O(3) | $M$—O(4) | $M$—O(1$^{i}$) | $M$—O(3$^{iii}$) | W—O(1) | W—O(2$^{ii}$) | W—O(3$^{v}$) | W—O(4$^{iv}$) | W—O(2$^{vi}$) | W—O(4$^{iii}$) |
| 75 | 2.187 (8) | 2.052 (8) | 2.241 (9) | 2.029 (9) | 2.070 (9) | 2.082 (9) | 1.823 (10) | 2.127 (9) | 1.814 (9) | 2.105 (10) | 1.876 (10) | 1.914 (10) |
| 70 | 2.155 (8) | 2.082 (8) | 2.305 (9) | 2.001 (9) | 2.077 (9) | 2.024 (9) | 1.821 (10) | 2.154 (9) | 1.816 (9) | 2.079 (10) | 1.887 (10) | 1.907 (10) |
| 65 | 2.116 (8) | 2.126 (8) | 2.345 (9) | 2.003 (9) | 2.066 (9) | 2.015 (9) | 1.803 (10) | 2.161 (10) | 1.817 (9) | 2.069 (10) | 1.860 (10) | 1.950 (10) |
| 60 | 2.105 (6) | 2.137 (7) | 2.380 (8) | 2.002 (7) | 2.058 (7) | 2.007 (8) | 1.784 (9) | 2.167 (9) | 1.819 (8) | 2.069 (9) | 1.867 (9) | 1.949 (9) |
| 55 | 2.113 (6) | 2.125 (7) | 2.405 (8) | 1.992 (7) | 2.061 (7) | 2.001 (8) | 1.772 (9) | 2.166 (8) | 1.819 (7) | 2.075 (8) | 1.876 (8) | 1.956 (8) |
| 45 | 2.077 (6) | 2.204 (7) | 2.427 (8) | 1.951 (7) | 2.006 (7) | 2.015 (8) | 1.818 (9) | 2.161 (7) | 1.808 (9) | 2.070 (7) | 1.857 (9) | 1.970 (9) |
| 40 | 2.090 (10) | 2.207 (10) | 2.420 (10) | 1.959 (10) | 2.031 (10) | 1.985 (10) | 1.776 (10) | 2.184 (6) | 1.809 (10) | 2.079 (10) | 1.854 (10) | 1.977 (10) |
| 35 | 2.053 (9) | 2.283 (9) | 2.409 (9) | 1.932 (9) | 2.004 (9) | 1.977 (9) | 1.845 (9) | 2.161 (6) | 1.819 (9) | 2.063 (9) | 1.840 (9) | 1.966 (9) |
| 30 | 2.041 (8) | 2.294 (8) | 2.402 (8) | 1.924 (8) | 2.006 (8) | 1.975 (8) | 1.844 (8) | 2.166 (5) | 1.818 (8) | 2.073 (8) | 1.829 (8) | 1.969 (8) |
| 25 | 2.031 (7) | 2.314 (7) | 2.430 (7) | 1.947 (7) | 1.994 (7) | 1.974 (7) | 1.837 (7) | 2.188 (5) | 1.783 (7) | 2.043 (7) | 1.825 (7) | 1.984 (7) |
| 20 | 2.039 (7) | 2.308 (7) | 2.439 (7) | 1.929 (7) | 2.000 (7) | 1.962 (7) | 1.839 (6) | 2.192 (5) | 1.796 (6) | 2.044 (6) | 1.835 (6) | 1.981 (6) |
| 15 | 2.025 (5) | 2.326 (6) | 2.435 (6) | 1.937 (6) | 1.988 (6) | 1.975 (6) | 1.845 (4) | 2.201 (6) | 1.777 (6) | 2.032 (6) | 1.826 (6) | 1.996 (6) |
| 10 | 2.028 (4) | 2.331 (5) | 2.447 (5) | 1.929 (5) | 1.984 (5) | 1.966 (5) | 1.850 (4) | 2.201 (5) | 1.786 (5) | 2.027 (5) | 1.834 (4) | 1.982 (5) |
| 5 | 2.010 (3) | 2.333 (4) | 2.448 (4) | 1.936 (4) | 1.981 (4) | 1.973 (4) | 1.854 (4) | 2.207 (4) | 1.774 (5) | 2.027 (5) | 1.818 (4) | 1.998 (5) |
| 0 | 2.010 (3) | 2.348 (4) | 2.446 (4) | 1.934 (4) | 1.980 (4) | 1.976 (4) | 1.850 (3) | 2.209 (4) | 1.768 (5) | 2.032 (5) | 1.822 (4) | 2.003 (5) |

* Numerical values of all the bond distances discussed here, and of quantities represented in the other graphs, have been deposited with the IUCr (Reference: HA0150). Copies may be obtained through The Managing Editor, International Union of Crystallography, 5 Abbey Square, Chester CH1 2HU, England.

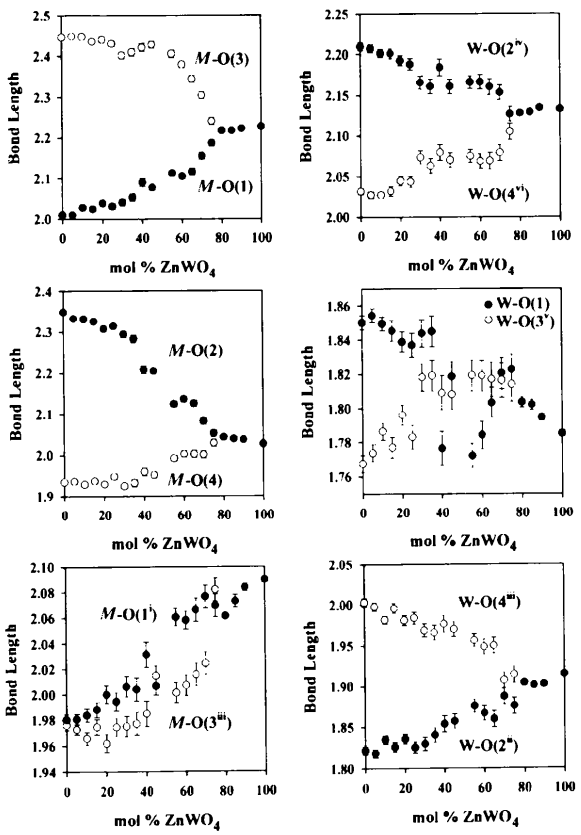


Fig. 7. Splitting of the $M$—O and $W$—O octahedral bond lengths (Å) across the solid solution, indicating a large excess increase in the $M$—O(2) bond length due to the transformation from monoclinic to triclinic. Symmetry operators for text and figures: (i) $1-x, 1-y, 1-z$; (ii) $-x, 1-y, 1-z$; (iii) $1-x, 1-y, -z$; (iv) $x, y-1, z$; (v) $x-1, y, z$; (vi) $x-1, y-1, z$.

decreases. This is in contrast to the other octahedral $M$—O or W—O bonds, which appear to remain essentially constant. Within the triclinic phases the $M$—O(1$^{i}$) and $M$—O(3$^{iii}$) bonds continue to decrease, such that a linear trend is evident across the entire solid solution. These two bonds run in the $ac$ plane and are principally responsible for the constant decrease in the $\beta$ angle, which occurs independently of the structural phase transition, as the Zn content increases.

As the active octahedra in the solid solution are the $MO_6$ octahedra, it can be assumed that chemical substitutions within these octahedra are responsible for the phase transition and that changes associated with the $WO_6$ octahedra occur as a secondary, induced process. Redfern, Bell, Henderson & Schofield (1995) showed that a microscopic atomistic order parameter for the triclinic phase may be defined from these symmetry-induced bond length changes. The $M$—O order parameter, which should be zero in the monoclinic phase, is defined as [$M$—O(3) + $M$—O(1$^{i}$) + $M$—O(2)] − [$M$—O(1) + $M$—O(3$^{iii}$) + $M$—O(4)] such that at the critical composition O(3) and O(1), O(1$^{i}$) and O(3$^{iii}$) and O(2) and O(4) become equivalent in the monoclinic structure. Fig. 8 shows that this atomistic order parameter behaves in a similar manner to the macroscopic order parameter and the phase transition is second-order with the order parameter conforming to the expression $Q \propto (X_c^* - X)^{\beta}$, where $\beta$ is the critical exponent and is equal to 1/2.

Further distortion of the octahedra may be assessed from the octahedral angle variance (Robinson, Gibbs & Ribbe, 1971) which is displayed in Fig. 9. The octahedral angle variance of the $MO_6$ octahedra increases as a function of Zn content up to approximately $(Cu_{0.15}Zn_{0.85})WO_4$ where it appears to plateau, the rate of increase decreasing at the critical composition. The $WO_6$ octahedron, on the other hand, shows no significant variation across the solid solution and no obvious inflection at the critical composition. This is not altogether unexpected as it is the $MO_6$ octahedra which are primarily affected in the phase transition with the $WO_6$ octahedra distorting as a secondary process.

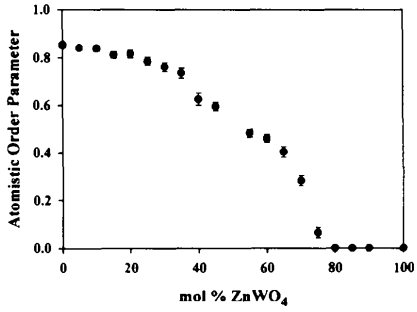


Fig. 8. Composition-dependent behaviour of the atomistic $M$—O order parameter calculated from [$M$—O(3) + $M$—O(1$^{i}$) + $M$—O(2)] − [$M$—O(1) + $M$—O(3$^{iii}$) + $M$—O(4)].

Perhaps a more meaningful parameter is the quadratic elongation of these octahedra (Robinson, Gibbs & Ribbe, 1971), which is shown as a function of composition in Fig. 10. There is a minimal decrease, on increasing Cu content, within the monoclinic phase in both sets of octahedra. Within the triclinic structures, however, the quadratic elongation of the $MO_6$ octahedra increases dramatically as the Cu content decreases,

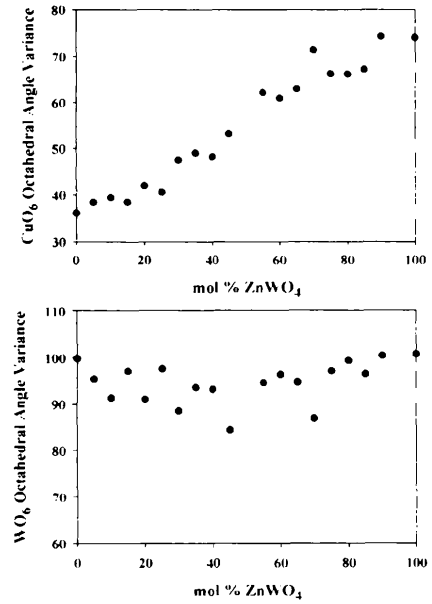


Fig. 9. Octahedral angle variance ( ) within the $MO_6$ and the $WO_6$ octahedra as a function of composition.

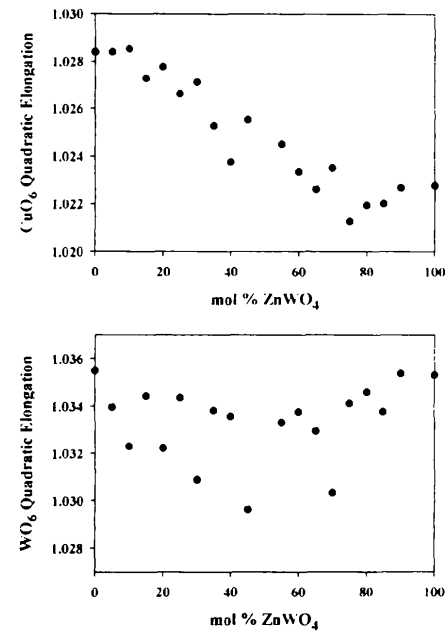


Fig. 10. Quadratic elongation of both the $MO_6$ and the $WO_6$ octahedra as a function of composition.

before apparently saturating at approximately $(Cu_{0.15}Zn_{0.85})WO_4$. The quadratic elongation of the $WO_6$ octahedra is not instantly affected at the critical composition and the triclinic distortion of the $MO_6$ octahedra does not induce a significant strain on the $WO_6$ octahedra until about $(Cu_{0.50}Zn_{0.50})WO_4$. As the distortion of the $MO_6$ octahedra continues to increase, the $WO_6$ themselves begin to distort, thus maintaining the basic structural integrity of the tungstates. It seems likely that the dominant effect of the Jahn–Teller elongation on the $CuO_6$ octahedra is therefore responsible for the slight increase in the $WO_6$ quadratic elongation at the Cu-rich end of the solid solution.

## 10. Conclusions

Rietveld analysis showed no evidence or justification for a lowering of the space-group symmetry (or a doubling of the cell size) within the intermediate samples of this solid solution and provided no further evidence for the nature of the two distinct electronic environments for Cu or the possibility of two $ZnO_6$ geometries. This indicates that there is no strong long-range correlation of the split $M$-site environments indicated by X-ray spectroscopy, and these are purely local effects whose random distribution preserves the average $P\bar{1}$ space-group symmetry. Analysis, assuming a single $M$ site, however, has enabled us to see how the microscope order parameters, particularly the atomistic $M$—O order parameter, reflect accurately the macroscopic spontaneous strain, resulting in the second order nature of the phase transition. It is also apparent that the non-symmetry-dependent strain component $e_{22}$ is associated with the Jahn–Teller effect upon the $M$—O(2) bond and that the linear decrease of the $\beta$ angle may be connected with the composition-dependent behaviour of the $M$—O($1^{i}$) and $M$—O($3^{iii}$) bonds. The driving force for the phase transition is clearly the Jahn–Teller distortion of the $Cu^{2+}$ cation environment.

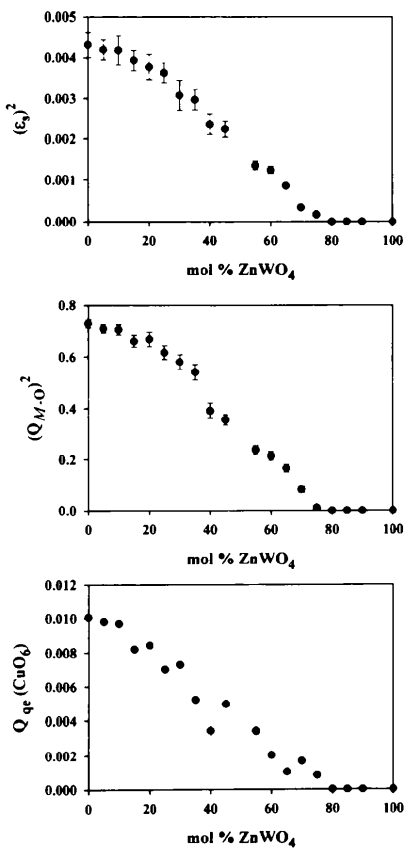


Fig. 11. Behaviour of the macroscopic strain and $M$-site strains as a function of composition, showing saturation of all order parameters close to the $CuWO_4$ end-member associated with a 'plateau effect'.

At the Cu-rich end of the solid solution there is a distinct deviation from that predicted by a second-order Landau model. Redfern & Schofield (1996) have shown from macroscopic strain measurements that this reflects a saturation of the order parameter in the range $(Cu_{1-x}Zn_x)WO_4$, where $0.12 \geq x \geq 0$, due to the short-range character of the strain field associated with the Zn atoms. This macroscopic plateau effect (Salje, 1995) should also be reflected in the microscopic behaviour in this region. Fig. 11 shows the square of the spontaneous strain plotted with the $M$—O order parameter squared. The deviation in both the macroscopic and atomistic order parameter from the second-order behaviour $[Q \propto (X_c^* - X)^{\beta}, (\beta = \frac{1}{2})]$ is obvious. The short interaction length of the strain fields associated with the Zn solute atoms is further demonstrated by the transition-related behaviour of the $MO_6$ quadratic elongation. This microscopic order parameter also saturates at approximately $(Cu_{0.88}Zn_{0.12})WO_4$, indicating that there is no overall long-range-correlated distortion of the $MO_6$ octahedra until the Zn solute atoms have reached a concentration capable of generating a homogeneous cooperative strain field.

## References

Arora, S. K. & Mathew, T. (1989). *Phys. Status Solidi A*, **116**, 405–413.

Arora, S. K., Mathew, T. & Batra, N. M. (1988). *J. Cryst. Growth*, **88**, 379–382.

Arora, S. K., Mathew, T. & Batra, N. M. (1989). *J. Phys. Chem. Solids*, **50**, 665–668.

Arora, S. K., Mathew, T. & Batra, N. M. (1990). *J. Phys. D*, **23**, 460–464.

Basu, A. K. & Sale, F. R. (1978). *J. Mater. Sci.* **13**, 2703–2711.

Basu, A. K. & Sale, F. R. (1979). *J. Mater. Sci.* **14**, 91–99.

Benko, F. A. & MacLaurin, C. L. (1982). *Mater. Res. Bull.* **17**, 133–136.

Bharati, R., Singh, R. A. & Yadava, Y. P. (1983). *J. Mater. Sci. Lett.* **2**, 623–624.

Brower, W. S. Jr (1970). *J. Appl. Phys.* **41**, 2266.
David, W. I. F., Ibberson, R. M. & Matthewman, J. C. (1992). Rutherford Appleton Laboratory Report No. RAL-92-032, Rutherford Appleton Laboratory, Didcot, England.
Doumerc, J. P., Dance, J. M., Chaminade, J. P., Pouchard, M. & Hagenmuller, P. (1981). *Mater. Res. Bull.* **16**, 985-990.
Filipenko, O. S., Pobedimskay, E. A. & Belov, N. V. (1968). *Sov. Phys. Crystallogr.* **13**, 127-129.
Foldvari, I., Capelletti, R., Kappers, L. A., Gilliam, O. R. & Watterich, A. (1989). *Phys. Lett. A*, **135**, 363-367.
Foldvari, I., Peter, A., Keszthelyi-Landori, S., Capelletti, R., Cravero, I. & Schmidt, F. (1986). *J. Cryst. Growth*, **79**, 714-719.
Forsyth, J. B., Wilkinson, C. & Zvyagin, A. I. (1991). *J. Phys. Condens. Matter*, **3**, 8433-8440.
Kihlborg, L. & Gebert, E. (1970). *Acta Cryst.* B**26**, 1020-1025.
Klein, S. & Weitzel, H. (1975). *J. Appl. Cryst.* **8**, 54-59.
Knight, K. S. (1992). *Mineral. Mag.* **56**, 399-409.
Mathew, T., Batra, N. M. & Arora, S. K. (1992). *J. Mater. Sci.* **27**, 4003-4008.
Moebius, H. H., Witzmann, H. & Harzer, D. (1963). *Z. Chem.* **3**, 157-158.
Pietro, B. di, Scrosati, B., Bonino, F. & Lazzari, M. (1979). *J. Electrochem. Soc.* **126**, 729-731.
Pisorevskii, Y. V., Sil'vestrova, I. M., Voszka, R., Peter, A., Foldvari, I. & Janszky, J. (1988). *Phys. Status Solidi A*, **107**, 161-164.
Redfern, S. A. T. (1993). *Phys. Rev. B*, **48**, 5761-5765.
Redfern, S. A. T. & Salje, E. K. H. (1987). *Phys. Chem. Miner.* **14**, 189-195.
Redfern, S. A. T. & Schofield, P. F. (1996). *Phase Transitions*. In the press.
Redfern, S. A. T., Bell, A. M. T., Henderson, C. M. B. & Schofield, P. F. (1995). *Eur. J. Mineral.* **7**, 1019-1028.
Robinson, K., Gibbs, G. V. & Ribbe, P. H. (1971). *Science*, **172**, 567-570.
Salje, E. K. H. (1995). *Eur. J. Mineral.* **7**, 791-806.
Schofield, P. F. & Redfern, S. A. T. (1992). *J. Phys. Condens. Matter*, **4**, 375-388.
Schofield, P. F. & Redfern, S. A. T. (1993). *J. Phys. Chem. Solids*, **54**, 161-170.
Schofield, P. F., Charnock, J. M., Cressey, G. & Henderson, C. M. B. (1994). *Mineral. Mag.* **58**, 185-199.
Schofield, P. F., Henderson, C. M. B., Redfern, S. A. T. & van der Laan, G. (1993). *Phys. Chem. Miner.* **20**, 375-381.
Schofield, P. F., Knight, K. S. & Cressey, G. (1996). *J. Mater. Sci.* **31**, 2873-2877.
Scott, J. F. (1968). *J. Chem. Phys.* **49**, 98-100.
Sears, V. F. (1992). *Neutron News*, **3**, 26-37.
Shapovalova, R. D., Belova, V. I., Zalesskii, A. V. & Gerasimov, Y. I. (1961). *Zh. Fiz. Khim.* **35**, 2713-2715.
Shoji, T. & Sasaki, N. (1978). *Min. Geol.* **28**, 397-404.
Smith, R. I., Hull, S. & Armstrong, A. R. (1994). *Mater. Sci. Forum*, **166-169**, 251-256.
Tyson, R. M., Hemphill, W. R. & Theisen, A. F. (1988). *Am. Mineral.* **73**, 1145-1154.
Wilson, C. C. (1995). *Neutron News*, **6**, 27-34.
Zhu, Y. C., Lu, J. G., Shao, Y. Y., Sun, H. S., Li, J., Wang, S. Y., Dong, B. Z. & Zheng, Z. P. (1986). *Nucl. Instrum. Methods Phys. Res. A*, **244**, 579-581.
Zvyagin, A. I. & Anders, A. G. (1974). *Sov. Phys. JETP*, **40**, 154-157.